Astron. Astrophys. Suppl. Ser. 92, 317-331 (1992)

ASTRONOMY & ASTROPHYSICS
SUPPLEMENT SERIES

Astron. Astrophys. Suppl. Ser. **92**, 317-331 (1992)

The ULYSSES energetic particle composition experiment EPAC

E. Keppler[1], J.B. Blake[2], D. Hovestadt[3], A. Korth[1], J. Quenby[4], G. Umlauft and J. Woch[5]

[1] Max-Planck-Institut für Aeronomie, Postfach 20, D-3411 Katlenburg-Lindau 3, Germany
[2] The Aerospace Corporation, Space Science Laboratory, Los Angeles, USA
[3] Max-Planck-Institut für Extraterrestrische Physik, Garching, Germany
[4] Imperial College of Science and Technology, Blackett Laboratory, London, UK
[5] Swedish Institute of Space Physics, Kiruna, Sweden

Received March 18; accepted July 5, 1991

Abstract. — The purpose of this paper is to briefly describe the EPAC investigation aboard the ULYSSES spacecraft. The EPAC sensor will measure the fluxes, angular distributions, energy spectra, and composition of ions in the energy range from 300 keV/nucleon to 25 MeV/nucleon. Some measurements will be shown obtained after turn-on in interplanetary space.

Key words: Sun: particle emission — instruments: miscellaneous — artificial satellites, space probes

1. Scientific objectives.

Lately it has become evident that measurements of the elemental composition of low-energy charged-particle populations in interplanetary space and the evolution in space and time of the composition are important for understanding dynamical processes such as accelaration, propagation, and modulation. It is well known that the proton-to-alpha particle ratio may vary by more than an order of magnitude during a given solar event. Ratios to heavier elements, e.g., Ne, Mg, Si or Fe, also may vary considerably during certain events. All these variations are observed typically below 5-10 MeV/nucleon, whereas at higher energies the elemental abundances in a flare are comparable to the elemental abundances in the solar corona of the solar atmosphere (Keppler *et al.* 1980). Special pre-acceleration / pre-enrichment processes, such as certain types of instabilities or stochastic Fermi acceleration processes have been suggested as the cause of these overabundances. However, different acceleration processes acting during the two main phases of a solar event, the flash- and the impulsive-phase, also could account for the observed composition variations; magnetic field merging at the flare site, or acceleration by shock waves propagating through the solar atmosphere have been proposed.

Once these particles are accelerated certain, as yet unknown, coronal structures may allow extended transport of the particles in the solar atmosphere in longitude and latitude, a temporary coronal storage of these particles, and a release onto open interplanetary magnetic field lines. As ULYSSES will reach high solar latitudes in 1993 and 1994, i.e. during solar minimum, these coronal structures may be limited to relative low solar latitudes at that time. Thus, the influence of various coronal structures upon coronal transport can be studied as well as the energy dependence of coronal storage, and finally the overall characteristics of interplanetary propagation of these particles at different heliographic latitudes. In connection with interplanetary propagation, it is also of great interest to study the influence of the interplanetary magnetic field and its fluctuations on particle propagation (diffusion), the effects of solar-wind streams (convection and adiabatic deceleration), the importance of gradient and curvature drifts, and the influence of the induced electric-field drift on low-energy particles, as all of these different "components" are expected to exhibit on average a rather strong, yet differing dependence on heliographic latitude.

Besides particles accelerated at the sun, there are interplanetary energetic particles that are accelerated in interplanetary space out of the thermal and suprathermal tails of the ion energy distributions by e.g. interplanetary-propagating shock waves or corotating interaction regions. Shock waves are able to accelerate particles directly and instantaneously via their induced electric field (gradient-drift mechanism) or slowly and cumulatively via a Fermi-type process acting between the shock front and the up-or downstream magnetic-field fluctuations and irregularities.

Send offprint requests to: E. Keppler.

Shock waves which propagate away from the flare site can accelerate particles at the sun and subsequently in the interplanetary medium. Intensity enhancements directly associated with the shock wave (shock spike events) or having some connection with the shock (ESP event) have been observed. Corotating interaction regions occur when fast solar-wind streams interact with slow ones. In this case isolated, yet extended, regions of enhanced magnetic field strength and fluctuations (co-rotating interaction regions) are formed; beyond about 3 AU even pairs of co-rotating shocks can occur. Interaction with these shock waves and/or with the co-rotating interaction regions expanding at a different speed to the ambient solar wind will result in acceleration of interplanetary particles. Only a detailed analysis of the time/intensity and time/anisotropy profiles of different ion species interacting with these interplanetary structures and phenomena will provide the necessary information on the prime acceleration mechanism(s).

Measurements of the quiet-time composition of energetic ions, performed in the ecliptic plane and during the high-latitude passages can provide information on the occurrence and latitudinal dependence of the "anomalous component" as well as on the penetration and streaming of galactic cosmic rays into the heliosphere. Taking the latitudinal dependence of the averaged Archimedean interplanetary magnetic field and the radial and latitudinal dependence of propagating, large-amplitude Alfvén waves into account, it has been shown that the radial mean free path increases with increasing heliographic latitude. This in turn means that particles from the outer part of the heliosphere, i.e. galactic cosmic rays or ionised and accelerated interstellar neutrals (the anomalous component ?) should penetrate into the inner heliosphere more effectively and more deeply over the solar polar regions than in the plane of the ecliptic, and that at the same time the cut-off energy for those particles being finally able to reach an observer located at 1-3 AU is far smaller over the poles than in the solar equatorial plane. With the EPAC instrument aboard the ULYSSES spacecraft we will have a singular opportunity to critically test these ideas. Because of the instrument's 4π-coverage, the importance and effectiveness of an out-of-ecliptic gradient drift on the different ion species could also be investigated.

2. Instrument design.

We use the $\mathrm{d}E/\mathrm{d}x, E$ technique, where particles traverse a thin detector and then stop it in a second, much thicker detector. Particles that traverse the two detector stack, are eliminated by a third "veto"- detector. Historically this technique permitted elemental separation above $\sim$ 1 MeV/ nucleon when semiconductor detectors were used. Lower energy thresholds were reached with thin-windowed proportional counters (Hovestadt *et al.* 1973) which lowered the $\sim$ 1 MeV/nucleon threshold for elemental resolution to a few 100 keV/nucleon. Disadvantages in complexity and mass led to the introduction of ultrathin silicon detectors of 5 μm and even 2 μm. While it is very difficult to fabricate such thin detectors by purely mechanical means, epitaxial structures of better homogeneity and better mechanical stability have become available and can be more easily produced.

Signal processing for such detectors includes the use of a charge-sensitive amplifier. The detector capacitance causes an increase in system noise. As a result, although very thin detectors are desirable in order to lower the threshold for two-parameter measurements, due to the noise increase with increasing capacitance, a compromise in the selection of detector thickness is required. We have adopted a detector thickness of 5 μm and a sensitive area of 25 mm, resulting in a 80 keV minimum detectable energy loss in such a detector. The calculated and measured (at the Lawrence Berkeley 88″ cyclotron) response of the combination of a 5 μm front detector (A) and a 100 μm back detector (B) is shown in Figure 1. A telescope based on such design will allow clear separation of H and He and heavier nuclei up to iron. The calculations mentioned above are based on the Northcliffe & Schilling range-energy tables (North-cliffe & Schilling 1970). At low energies, the values are interpolated according to $(\mathrm{d}E/\mathrm{d}x) \sim \sqrt{E}$. Also nuclear losses were included by applying the "universal" curve published by Lindhard *et al.* (1963). We have also calculated energy losses of heavy particles in detector material and have compared them to actual measurements. We have found good agreement between our measurements and the calculations.

Each telescope consists of three Si-surface barrier detectors, A, B, and C (see Tab. 1) surrounded by a massive platinum shield. Background rejection is realised by using multiparameter analysis. All four telescopes operate in a self-calibrating $\mathrm{d}E/\mathrm{d}x$ (detector A) *versus* E (detector B) mode, wherein particle tracks can be used to obtain conclusive absolute calibrations. Each telescope and associated electronics is able to measure the elemental composition of low-energy nuclei from hydrogen to iron. Each telescope has a geometric factor of about 0.08 $\mathrm{cm}^2\mathrm{sr}$. The EPAC experiment (Fig. 2) consists of four such telescopes (T1-T4), which are mounted such that their central axes include angles of 22.5°, 67.5°, 112.5° and 157.5°, with respect to the spacecraft spin axis. Each telescope has a field-of-view with a full angle of 35°. Thus the instrument covers 80% of the full sphere during one spacecraft rotation.

The front detectors (A) are protected against sunlight by Al-layers, 80 $\mu\mathrm{g}/\mathrm{cm}^2$ thick, and are used with the Al-side facing the incoming particles. The B-detectors are installed with their Au-side facing the front detector to minimize radiation damage. The weight and power budget

of the instrument is summarised in Table 2. Figure 3 is a picture of the instrument.

3. The analogue signal-processing concept.

The design of the instrument's electronic system was dictated by severe weight and power restrictions. In several respects, new approaches had to be developed, established and qualified. Figure 4 shows the block diagram of the analogue circuitry of the instrument. Charge-sensitive preamplifiers are used following each detector, with subsequent differentiation/integration (time constant: 0.3 μs). Output pulse amplification employs baseline restorers with a reaction time of a few microseconds. Discriminators provide the coincidence/anticoincidence signals required for data classification and for several rate channels. Technical details of some special features are discussed elsewhere (Keppler *et al.* 1981).

The various signal lines are combined into linear Analogue-OR amplifiers, to form an event-controlled multiplexing scheme, which suppresses the noise of all inactive channels; only the active channel is amplified. Simultaneous presence of two or more signals causes a logic inhibit. All these devices have been developed as hydrids; they are radiation-hard up to $\approx$ 200 krad (Si).

Three types of analogue-to-digital-conversion are utilised in this instrument: The E and the $\mathrm{d}E/\mathrm{d}x$ signals are digitized in a fast 8-bit Analogue-to-Digital Converter (ADC). Proton- and low-energy-ion spectra are obtained from 3-bit Pulse-Height Analyser (PHA) (Keppler *et al.* 1978), made up of nine discrete pulse-amplitude discriminators. For housekeeping purposes, another 8-bit ADC is used.

Coincidences are derived from dicriminators. Valid conditions are evaluated by fast LP-Schottky logic which within 0.1 μs after signal settling (which is less than 0.4 μs) and generate a "Power ON" signal. Signals are further processed in (slower) CMOS logic. Events, where more than one telescope responds, are ignored.

In the absence of events, the ADC, and its clock are turned off. These circuits are turned on only if the "Power ON" signal, mentioned above, appears. A short time after this a first "Start Conversion" signal is generated, which causes the ADC to analyse the input signal. Only single telescope response is accepted. The ADC is turned off after each analysis. An ion, recorded by a telescope, causes an "event"; the information associated with it is checked and then coded into a 24-bit string.

Due to the large dynamic range in the B-channel (up to 100 MeV), it is split into two branches, low (90 keV/channel) and high (390 keV/channel). The branch to be evaluated is selected automatically with the help of a special discriminator. The A signals is resolved in Heavy-Ion Mode (HMOD) into 90 keV/channel and in Ion Mode (IMOD) into 45 keV/channel. Mode-selection is made by telecommand.

4. Operational aspects, data frame and status verification.

Various data categories are generated from the counting rates of the detectors. Sectored rates are derived from the spin period clock of the spacecraft. An "Ion Mode" and a "Heavy Ion Mode" can be commanded; data may also be taken from one telescope exclusively or devoted to one "species" (one element group) only (see below). The instrument operates continuously whichever mode is selected, and its status is transmitted in "Status Words". The full information on measured single particle events is contained in a 24-bit event string. Data are organized to form the Experiment data Frame (EDF, Fig. 5), which assigns about 19% of the data stream to event strings, 1% to status information, 15% to rates, and 65% to spectrally and directionally resolved data for protons, low-energy ions ($Z \geq 1$) and four different heavy-ion groups.

In the course of the mission, the viewing directions of the telescopes, which are fixed in the spacecraft frame of reference (Fig. 6), move across the sky.

After bitrate-changes the instrument-sequences are maintained; measuring time are changed correspondingly.

After turn-on, information, stored in PROMs, is read into RAMs and transmitted within the first two EDF's, the PROMs will be turned off after readout. The contents of the RAMs can be changed by command, RAM readouts may be initiated any time by command.

Two SYNC-words identify the EDF, two other words contain the number of transmitted EDFs; overflow will not occur within 2 years.

At a late stage we provided means to include the GAS-instrument (see Witte *et al.*, this issue) into the payload. This instrument had been part of the payload of the US-spacecraft, which was cancelled. We offered to let the GAS-instrument use a fraction of our data stream for certain time periods. Commanding to that instrument became possible by using 16 bit command words which differed in the first and second 8 bit half word.

5. Data categories.

The instrument generates 12 different classes of data, summarized in Table 4; time, energy and directional resolutions are also given.

All events are categorised by their $(\mathrm{d}E/\mathrm{d}x)-$ signal into three crude classes; their respective numbers are transmitted from three event memories. So besides the 32 event strings we also get per EDF the total number of events recorded during that time interval.

Less detailed information on energy spectra are obtained with higher time resolution from 4 groups of ions. 8 energy channels are formed for each group. Bands, corresponding to the $(dE/dx - E)$ tracks are stored in a RAM look-up table. All events are sorted accordingly for 4 ion groups (He, C-N-O, S-group, F-group). For telescopes 2 and 3 these are in addition resolved into 8 spin-sectors. A full set will be transmitted in about 34 min. If only one species is selected, time resolution increases to $\sim$ 8.5 min.

Protons are identified separately in 8 channels (3-bit PHA) using the B-detector outputs (500 keV to 1.6 MeV). All channels are resolved into eight sectors.

From the A-detector's output, integral fluxes of ions are obtained. Contributions will come from ions above an energy, defined by dead-layer thickness and electronic threshold of about 145 keV. Contribution from electrons scattered through large angles may contribute to the lowest channel, but as the detector thickness corresponds to the range of $\sim$ 25 keV electrons, its electron detection efficiency is certainly $\ll 1$.

The 4 A-detector outputs are connected to the PHA through a multiplexer (as are the B-detectors, see Fig. 4). The thresholds of the PHA (see Tab. 6) are adjusted such, that in "High Gain"-Mode channel 1 to 3 "protons" ($Z \geq 1$), in channel 4 to 5 "α-particles" (i.e. $Z \geq 2$), in channel 6-8 "oxygen" (i.e. $Z \geq 6$) is detected. In "Low-Gain", the passbands are shifted one channel up: channel 1 and 2 record now $Z \geq 1$, channels 3 to 4 $Z \geq 2$, channels 5 to 7 $Z \geq 6$ and channel 8 $Z \geq 10$ particles. The latter corresponds to about 500 keV/nucleon. This class of data is obtained in 16 min.

Much higher time resolution is obtained from rates, which correspond to the integral over energy of the proton- and the $Z \geq 1$ spectra. Telescopes 2 and 3 are resolved in eight sectors.

The solar aspect angle varies in the course of the mission from $\sim$ 90° after launch to less than 11.5° at Jupiter. It will again increase during polar passage. This means, that there will be periods, when telescopes 1 or 2 will be fully illuminated by the sun and might affect the $Z \geq 1$ data, but not coincidence rates.

Two electron channels corresponding to 100 keV $\leq E \lesssim 0.4$ MeV and to $E \gtrsim 0.3$ MeV are also formed for each telescope. These channels are defined from proper combination of dicriminator thresholds. Their energy range is, however, not very accurately defined (due to electron scattering). For heavy ions there are also 16 rate channels for each of the 4 telescopes and each of the 4 species. They are read out once every 8 minutes.

For each telescope the background rates of detector B and C are transmitted, each accumulated over 4 minutes. The equivalent geometrical factor is $F_B = 1.60$ cm^2 and $F_C = 6.02$ cm^2. For coincidence rates of all 3 detectors the geometrical factor $G = 0.08$ cm^2 ster applies.

6. Inflight test and ground calibration.

An inflight calibration is achieved naturally by the $E - dE/dx$ signatures of the various nuclei contained in the ambient radiation. For functional performance tests we have incorporated a pulse generator, which on command produces sequences of coincident and noncoincident pulses. This set generates a repetitive pattern, which is suitable for checking the coincidence/anticoincidence conditions within the instrument; it also simulates some data categories.

On the ground, calibration was performed by measurements made at the Lawrence Berkeley 88″ cyclotron and at the LANL Heavy Ion van de Graaff in Los Alamos (see Fig. 1). The telescopes have also been irradiated at CERN with 600 MeV protons, and at JPL with a simulated RTG source in order to investigate background susceptibility. This was repeated prior to launch, when the RTG was moved to the S/C and the experiments were operated, so that background rates could be determined. Turn-on in flight occurred during a relative quiet period, so that background rates could be determined. Background rates for all coincidence channels are Ø, single rates for the B- and C-detectors in flight match those during RTG-tests on ground very well.

Functional performance was tested with the help of an appropriate checkout facility (Umlauft & Keppler 1978). This equipment could be also connected to the spacecraft checkout computer and was used during system checkout as well. During flight, the same equipment is used for quick-look access to the experiment data.

7. Performances in space.

The sensor was designed to operate at a temperature of $\sim$ + 10°c near Earth. This temperature was expected to drop to below − 20°C at Jupiter. After instrument turn-on the sensor temperature leveled off at + 9.5°C, while the electronic box operated at T $\sim$ +37°C; in 2 AU distance the sensor temperature had dropped to −25°C, as expected. Figure 7 shows 24 hours of housekeeping data after turn-on (temperatures in sensor and electronic box, total current, and several supply voltages). The stability is perfect, current reading is as expected.

Soon after turn-on, energetic particles arrived at ULYSSES. W shall not discuss the observations with respect to their physical meaning, but display some observations as a demonstration of the instrument's capabilities.

The instrument was first turned on on October 19, 1990. Checkout took place during October 20-21, 1990. Through all other periods the instrument remained operating.

Figure 8 shows triple coincidence channels, corresponding to $E_p > 3.4$ MeV, for T1 to T4 and an electron channel during this period.

Detector A in telescope 3 became noisy soon after turn-on, but remained functioning since; its noise affected only a few data channels. The background levels in the B- and C- detectors are of course determined by the RTG gamma radiation, which, however, did not affect the A-detectors, and from penetrating particles with energies above 35 MeV (if protons), corresponding to the thickness of the platinum shield.

The angle between spin axis and the direction to the sun remained close to 90 degrees during this first period. As a consequence some of the low energy ion data (ZS) of telescope 2 and 3 are affected by sunlight, which is difficult to judge. However, such condition will never occur during the rest of the mission. When the spacecraft passed beyond 2 AU away from the sun, none of the channels was affected by light anymore.

Figures 8 to 10 show plots of different channels for the same period (October 23 to 29, hourly averages). Electrons were seen to rise simultaneously in all 4 telescopes on October 23, 1990, at 08:37 UT, several hours earlier than protons appeared ($\sim$ 17 UT). Two p-channels from T1-T4 are shown in Figure 9 (see also Tab. 5). It can be seen, that higher energetic protons arrived earlier than the lower energetic particles (dispersion). Figure 10 shows for T1, T2, and T4 the response to different ions: Protons, α-particles and oxygen; these channels have about the same energy/nucleon ranges. While there are only weak fluxes of heavier ions present, α-particles were seen in fluxes comparable to those of protons. Figures 11 shows proton spectra obtained in the 4 telescopes on subsequent days. While the data shown in Figures 8 to 10 represent hourly averages, Figure 11 is drawn from daily averages, Figure 12 finally shows events collected by the 4 telescopes during the whole period. The lower track is due to He (protons are excluded), C-N-O tracks may also clearly be seen, and some heavier material, (Ne, Mg, etc.) The large energy-events in the upper right are due to iron. Each point included in the diagrams (total of about 50 000) carries with it still directional information, i.e. the data could be also drawn associated with directions in space.

Acknowledgements.

We are indebted to many individuals who have contributed to the EPAC experiment. The untiring excellent work of the staff of MPAE-Lindau, in particular K. Fischer, W. Engelhardt, V. Thiel, A. Fröhlich, H.A. Heinrichs, and H.P. Winterhoff, was a crucial part of preparing EPAC for spaceflight. We thank Dr. W. Weiβ for many helpful discussions. Mr. Sam Immamoto of the Aerospace Corporation ably supported calibration efforts. We thank Prof. W. Klein, Dr. W. Winkelnkemper, and Dr. A. Glasmachers, of the University Bochum, for their contribution in evaluating the electronic design. G. Funke, of Valvo, Hamburg, and J. Bourman, of the ESA Space Science Department at ESTEC, who helped us with hybrid technology. We greatfully acknowledge the work of Prof. Wagemann and Dr. Bräunig, of Hahn-Meitner-Institut Berlin, for valuable advice and technical support during radiation hardness testing of some of our electronic components. We thank Dr. Delfs and Dipl.-Phys. Küchler from Rohde & Schwarz, München, and GMD, Bochum, who manufactured the hybrid elements. The flight electronics were fabricated at Dornier -System GmbH, Friedrichshafen. We appreciate the help and cooperation of Drs. T.A. Fritz and R. Belian of the Los Alamos Scientific Laboratory for their support in carring out testing using the LANL heavy-ion van de Graaff.

References

Hovestadt D., Vollmer O., Gloeckler G., Fan C.Y. 1973, Proc. 13th Int. Cosmic Ray Conf., p.1498

Keppler E., Wilken B., Umlauft G., Fischer H., Williams D.J., Richter K., Bubla E., Fischer K. 1978, Forschungsberichte des BMFT, BMFT-FB W 78-19

Keppler E. 1980, Phil. Trans. Royal Society, London, A297, 621

Keppler E., Glasmachers A., Winkelnkemper W., 1981, IEEE Trans., IM-30, No. 3, 177

Lindhard J., Nielsen V., Scharff M., Thomsen P.V. 1963, Mat Fys Medd Dan Vid Selsk, 33, No. 14, 1

Northcliffe L.C., Schilling R.F. 1970, Nuclear Data Tables, A7, 233

Umlauft G., Keppler E. 1978, IEE Trans., NS-25, No.6, 1640

TABLE 1. *Detector dimensions (T1-T4).*

Detector	Area [mm^2]	Thickness [μm]	Operating voltage [V]	Leakage current (typical) [μA]	Comments
A	25	5	10	1	Epitaxial
B	80	100	30	0.5	Surface barrier
C	300	300	70	0.5	Surface barrier

TABLE 2. *Weight and power budget.*

	Weight [g]	Power consumption [mW]
SENSOR	542	220
Heater	10	500[1]
ELECTRONIC BOX	2143	3210
EXPERIMENT TOTAL (without Heater)	2685	3430 (123 mA at 28V, +20°C)

[1] Additional power provided for heating, if required.

TABLE 3. *Discriminator settings (electrical).*

	A_{i1}		A_{i2}	B_{i1}	B_{i2}	B_{i3}	C_i	
Discriminator	Low	High					Low	High
Threshold energy [keV]	165	280	420	35	95	1990	70	88

Low/high selection by telecommand.

TABLE 4. *Data categories.*

Particle type	Acronym	Telescope	Number of sectors*	Energy range MeV/amu	Number of energy channels	On-board classification	Time for one data set**	
Protons	PS	1-4	8	0.5-1.5	8	–	17	min
	PR	2, 3	8	0.5-1.5	1	–	512	s
	OP	1-4	1	0.5-1.5	1	–	128	s
Ions $Z \geq 1$	ZS	1-4	8	0.1-0.5	8	–	17	min
	ZR	2.3	8	0.1-0.5	1	–	512	s
	OZ	1	4	0.1-0.5	1	–	128	s
		2, 3, 4	1	0.1-0.5	1	–	64	s
Electrons	ELL	1-4	1	0.1...0.4	1	–	128	s
	ELH	1-4	1	> 0.3	1	–	128	s
Heavy ions	HS	1-4	4	0.4-4	8	4	34	min
He, O, S, Fe	HR	1-4	1	0.4-4	1	4	512	s
	ER	1-4	1	0.4-4	1	3	256	s
Background	BR	1-4	1	N.A.	3	–	1024	s
single events	EV	1-4	4		256	–	32 events/256 s	

* '1' means sum over complete spin; number of spin revolutions according to time resolution different for different categories.

** For 1024 bit/s spacecraft bit rate.

TABLE 5. *PHA thresholds.*

Protons[1] Channels			Energy band[1] A1 Low[2]				Energy band[1] A1 High[2]			
#	[keV]	ΔE [keV]		#	[keV/amu]	ΔE [keV/amu]		#	[keV/amu]	ΔE [keV/amu]
1	508- 520	12	$Z \geq 1$	1	204-262	58	$Z \geq 1$	1	311-432	121
2	520- 541	21		2	262-441	179		2	432-508	76
3	541- 574	33		3	441-508	67				
4	574- 629	55	$Z \geq 2$	4	196-291	95	$Z \geq 2$	3	191-295	104
5	629- 768	139		5	291-422	131		4	295-422	127
6	768- 990	222	$Z \geq 6$	6	201-289	88	$Z \geq 6$	5	183-291	108
7	990-1423	433		7	289-449	160		6	291-436	145
8	1423-1559	136		8	449-494	45		7	436-493	57
							$Z \geq 10$	8	451-516	65

[1] Slightly different for different telescopes.
[2] Discriminator thresholds for detectors A.

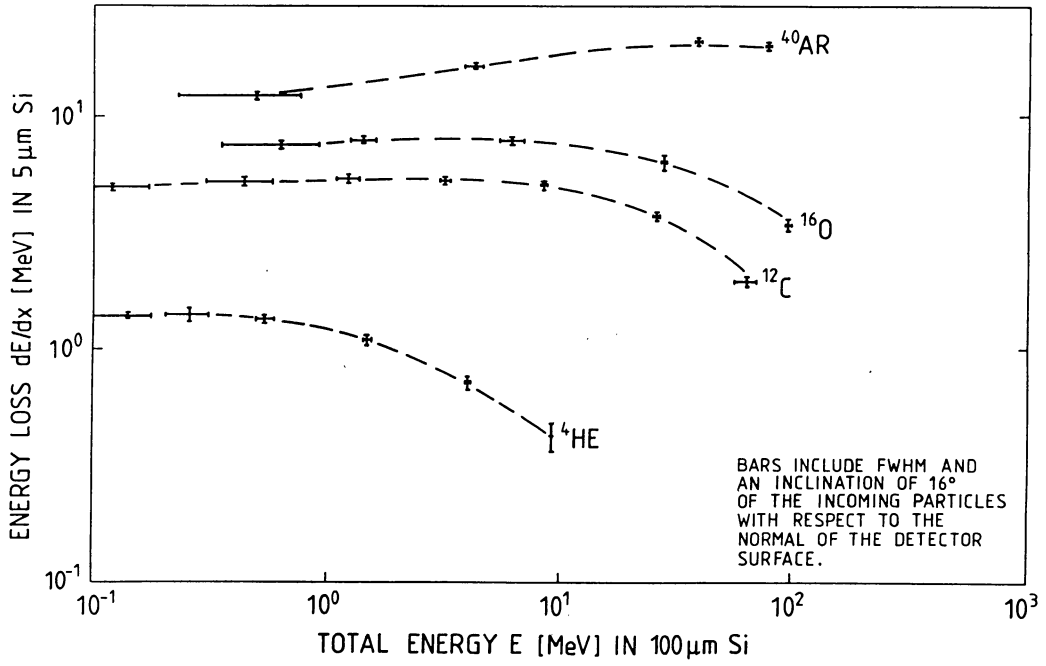

FIGURE 1. Energy losses of heavy ions (He, C, O, Ar) in frony- and black-detectors of a space telescope. Measurements were performed at the LBL Cyclotron in Berkeley.

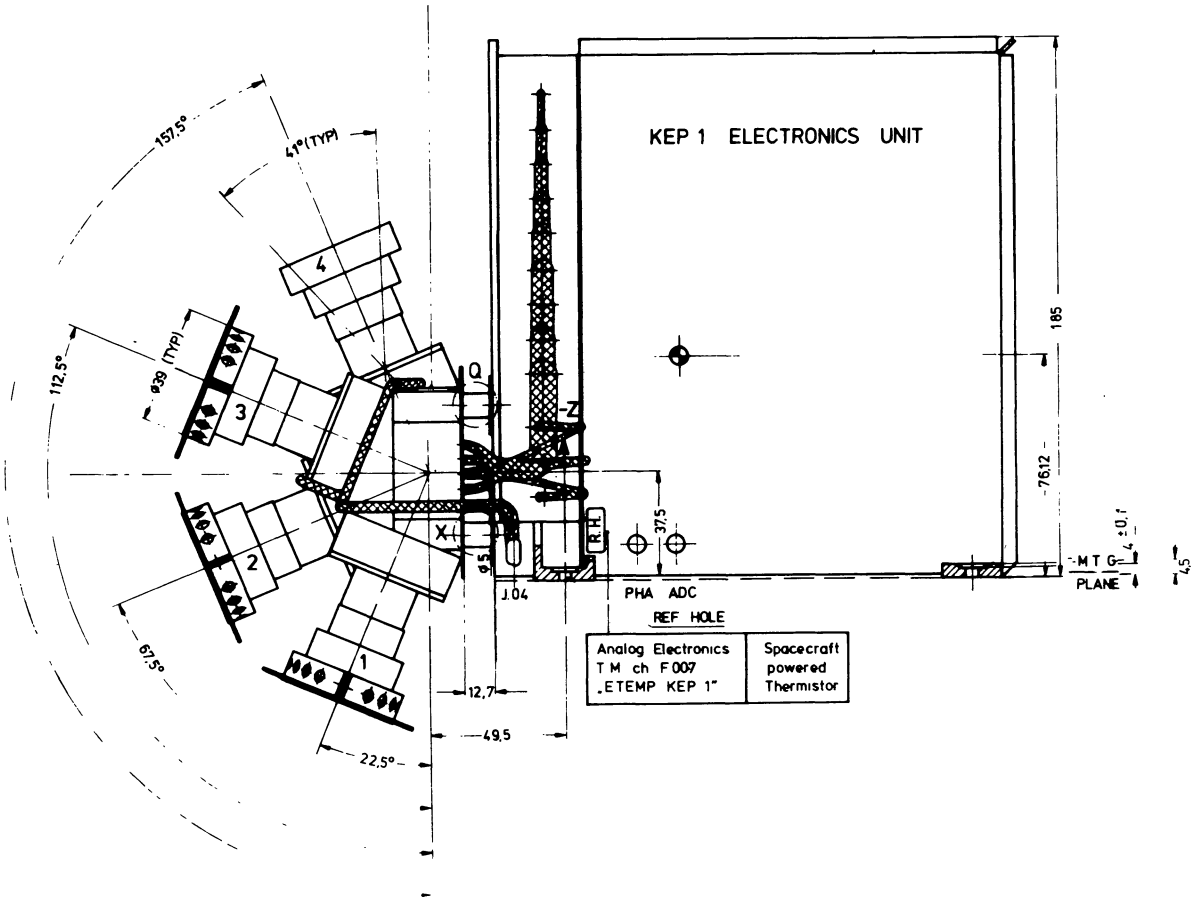

FIGURE 2. Cross section through EPAC telescopes, attached to electronic box.

FIGURE 3. View on the instrument. Telescopes are still closed by protective covers. Telescope 1 is viewing upwards, telescope 4 downwards.

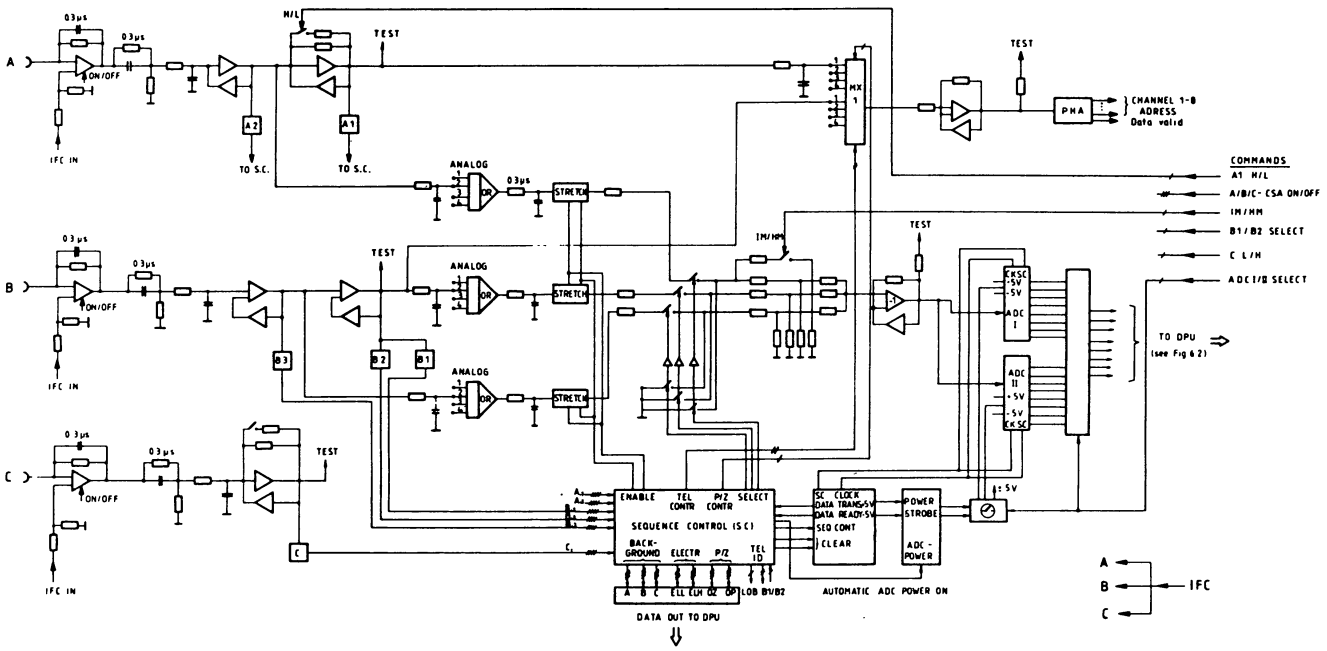

FIGURE 4. Electronic block diagram, showing one telescope only. The other 3 telescopes are identical and connected to the multiplexer inputs which are numbered (1-4).

EDF 0..7 | 8..15	FRAME TLM FORMT	Ø	1 2 3 ΔE E ID	4 5 T2 T3	6 T1	7	8 9 10 11 12 13 14 15 TX S1 S2 S3 S4	16	17 18 19 ΔE E ID	20 21 22 23 TX Q1 Q3	24 25 26 27 28 29 30 31 TX S5 S6 S7 S8	1024 BPS (SEC)	128 BPS (SEC)	LINE 3 TX
PART ON LINE 1 | PART ON LINE 2	Ø	SYØ		S1 S1	Q1	T2	E1--- ----- ----- -----	T1		E1--- -----	E1--- ----- ----- -----	32	256	IDX
	1	T4	ID	S5 S5	Q3	T3	E2--- ----- 16 BIT-----	T2		E2--- -----	E2--- ----16 Bit -----	64	512	TLM
	2	EC1		S2 S2	Q2	T2	E3--- ----- ----- -----	T3		E3--- -----	E3--- ----- ----- -----	96	768	ECØ
	3	T4	EV	S6 S6 (ZR)	Q4 (OZ)	T3 (OZ)	E4--- ----- ----- ----- (ZS)	T4 (OP)	EV	E4--- ----- (HS)	E4--- ----- ----- ----- (ZS)	128	1Ø24	MOD
	4	CS1		S3 S3	Q1	T2	E5--- ----- ----- -----	T1		E5--- -----	E5--- ----- ----- -----	16Ø	128Ø	RST
	5	T4	OZ	S7 S7	Q3	T3	E6--- ----- ----- -----	T2		E6--- -----	E6--- ----- ----- -----	192	1536	BRA
	6	CS2		S4 S4	Q2	T2	E7--- ----- ----- -----	T3		E7--- -----	E7--- ----- ----- -----	224	1792	BRB
	7	T4		S8 S8	Q4	T3	E8--- ----- ----- -----	T4		E8--- -----	E8--- ----- ----- -----	256	2Ø48	BRC
					TX					Q2 Q4				
PART ON LINE 2 | PART ON LINE 1	Ø	SY1		S1 S1	E1---	E1---	----- ----- -----	T1		E1--- -----	E1--- ----- ----- -----	32	256	
	1	ELH	EL	S5 S5	E2---	E2---	-----16 Bit -----	T2		E2--- -----	E2--- -----16 Bit -----	64	512	
	2	ERL		S2 S2	E3---	E3---	----- ----- -----	T3		E3--- -----	E3--- ----- ----- -----	96	768	ID
	3	ELL	EV	S6 S6 (PR)	E4--- (HS)	E4---	----- ----- (PS)	T4 (HR)	EV	E4--- ----- (HS)	E4--- ----- ----- ----- (PS)	128	1Ø24	
	4	ERM		S3 S3	E5---	E5---	----- ----- -----	T1		E5--- -----	E5--- ----- ----- -----	16Ø	128Ø	
	5	ELH	ER	S7 S7	E6---	E6---	----- ----- -----	T2		E6--- -----	E6--- ----- ----- -----	192	1536	BR
	6	ERH		S4 S4	E7---	E7---	----- ----- -----	T3		E7--- -----	E7--- ----- ----- -----	224	1792	
	7	ELL		S8 S8	E8---	E8---	----- ----- -----	T4		E8--- -----	E8--- ----- ----- -----	256	2Ø48	
												4.2	34.1	MIN

FIGURE 5. The Experiment Data Frame (EDF) shows how the data are organized and submultiplexed. The upper and the lower part are transmitted through different lines to the S/C, the content is interchanged after 8 EDF's. A third line, shown on the right side, contains status information and background rates.

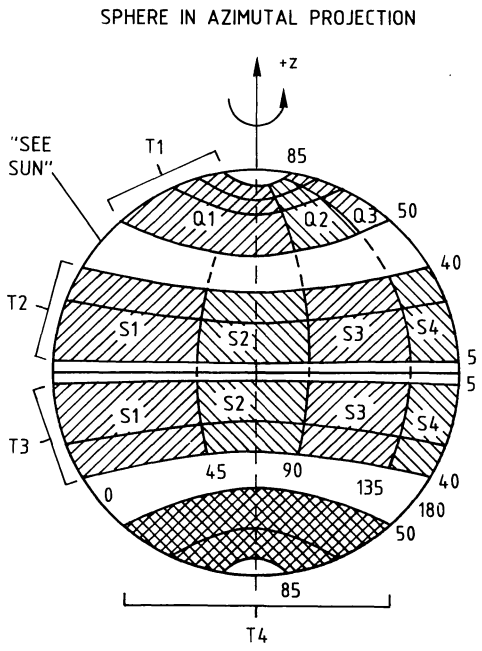

FIGURE 6. Sketch of the segments of the sphere covered by the four telescopes.

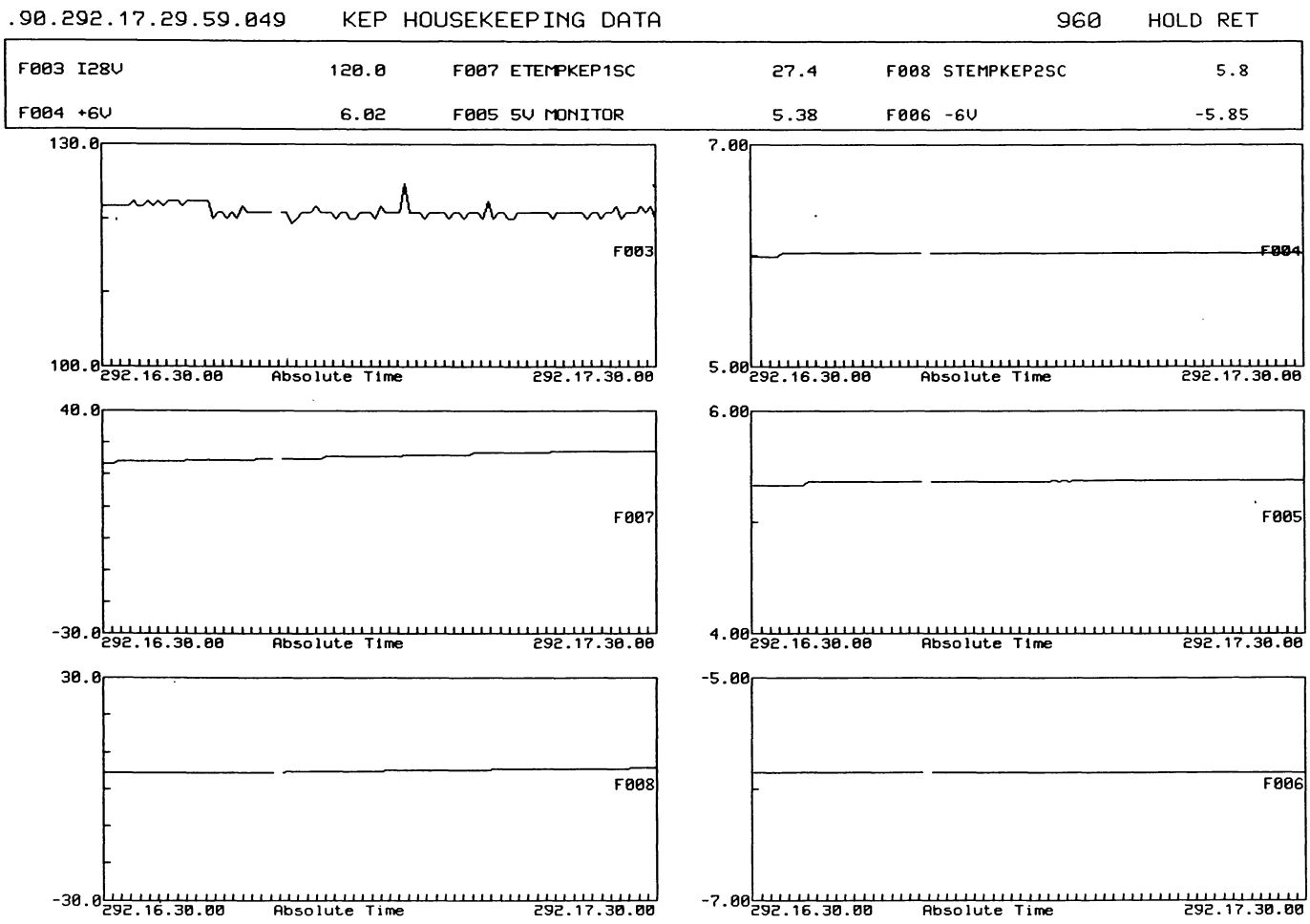

FIGURE 7. This figure shows a summary of housekeeping values after turn-on. Channels F007 and F008 represent the temperatures in the electronic box and the sensor, respectively. Channel F003 is the full current drawn by the instrument. On the right side, internal voltages ate shown.

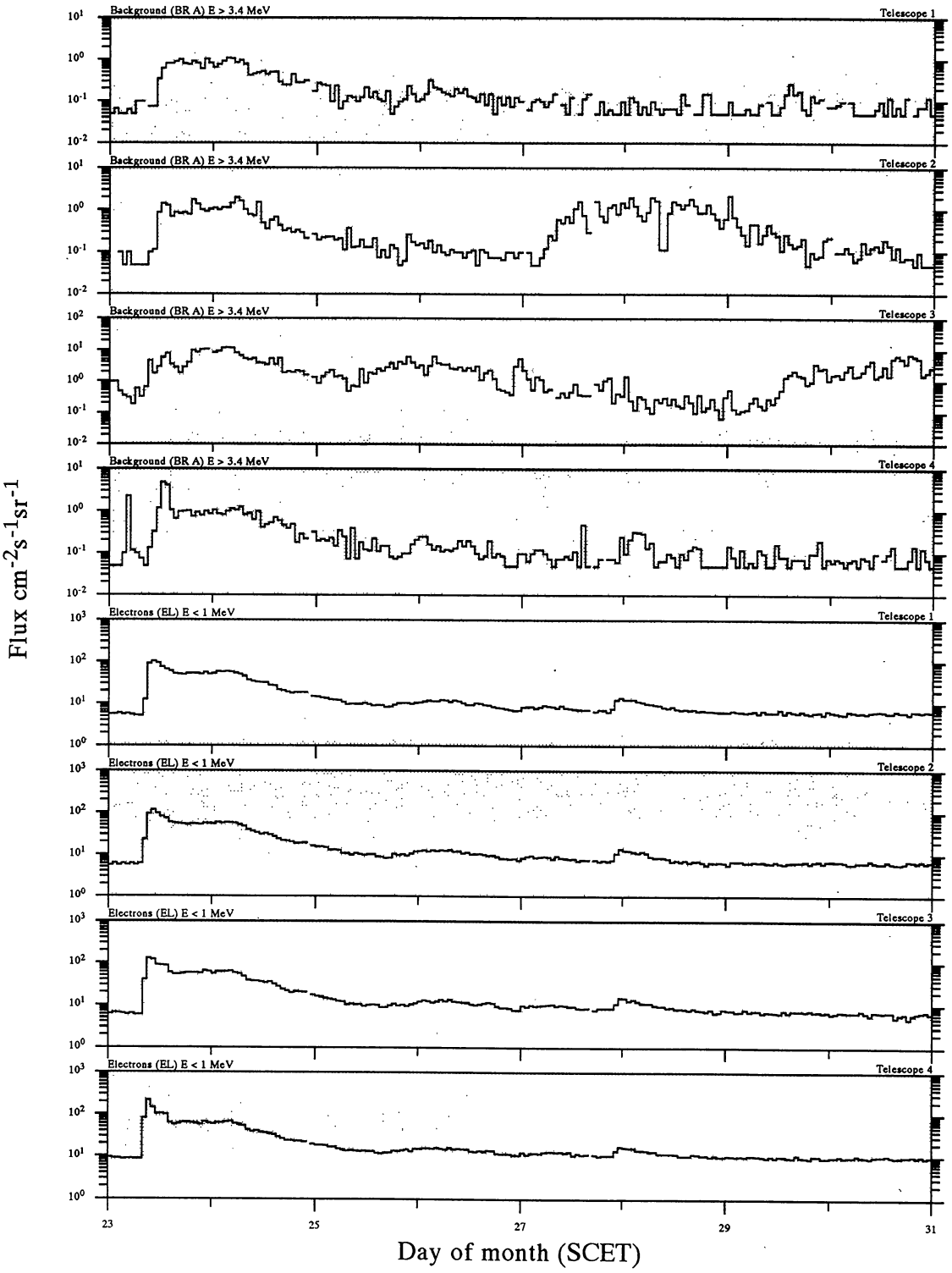

FIGURE 8. Triple coincidence channels ($E_p > 3.4$ MeV) for T1-T4 (hourly means) are shown in panels 1 to 4 (from top) along with electron channels ($0.1 < E_e < 1$ MeV) in panel 5 to 8 for T1 to T4.

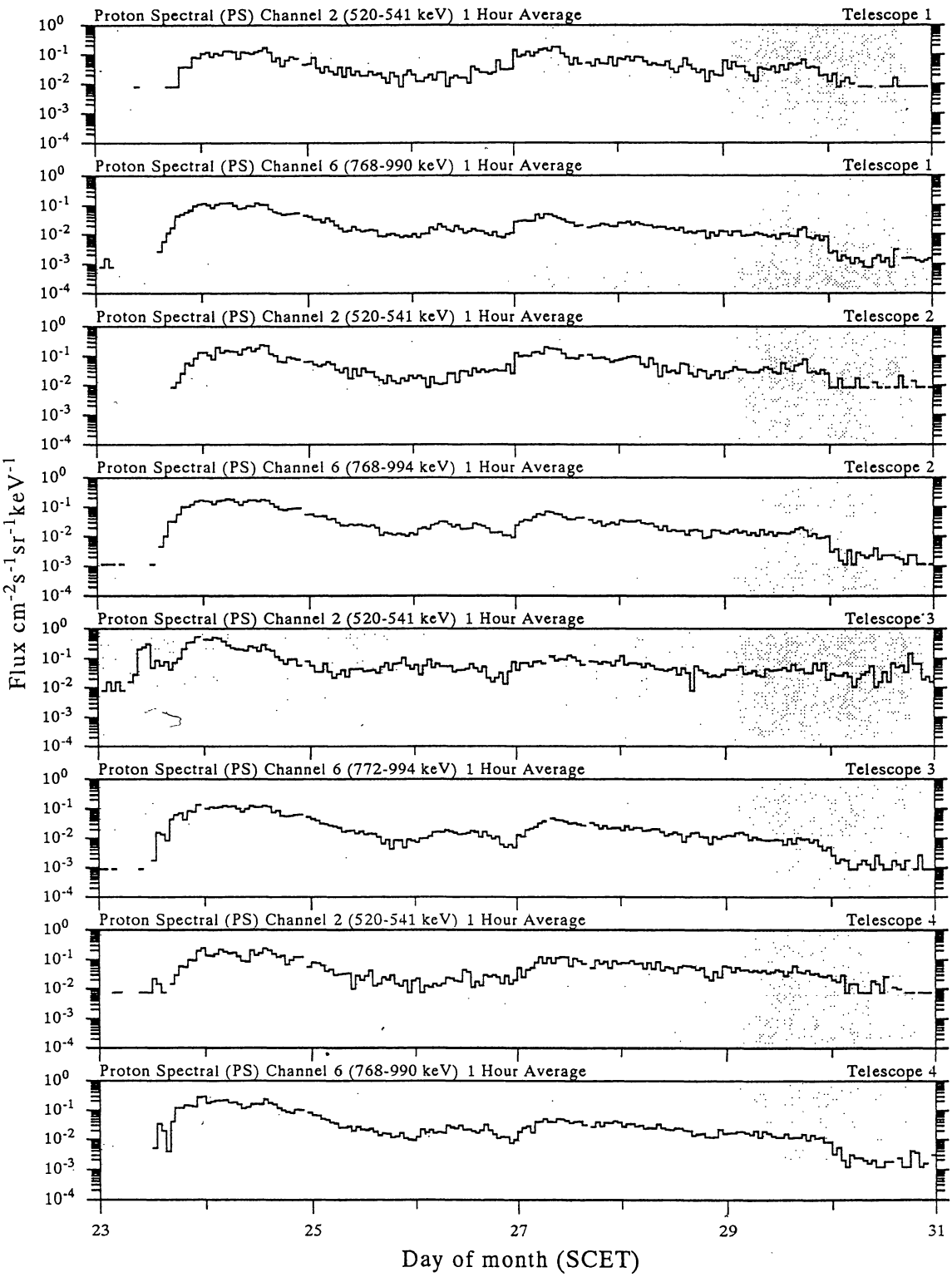

FIGURE 9. Protons of energy 520-541 keV and 768-994 keV are shown for all 4 telescopes (panel 1 and 2 for T1, panel 3 and 4 for T2, etc.) Hourly averages are shown.

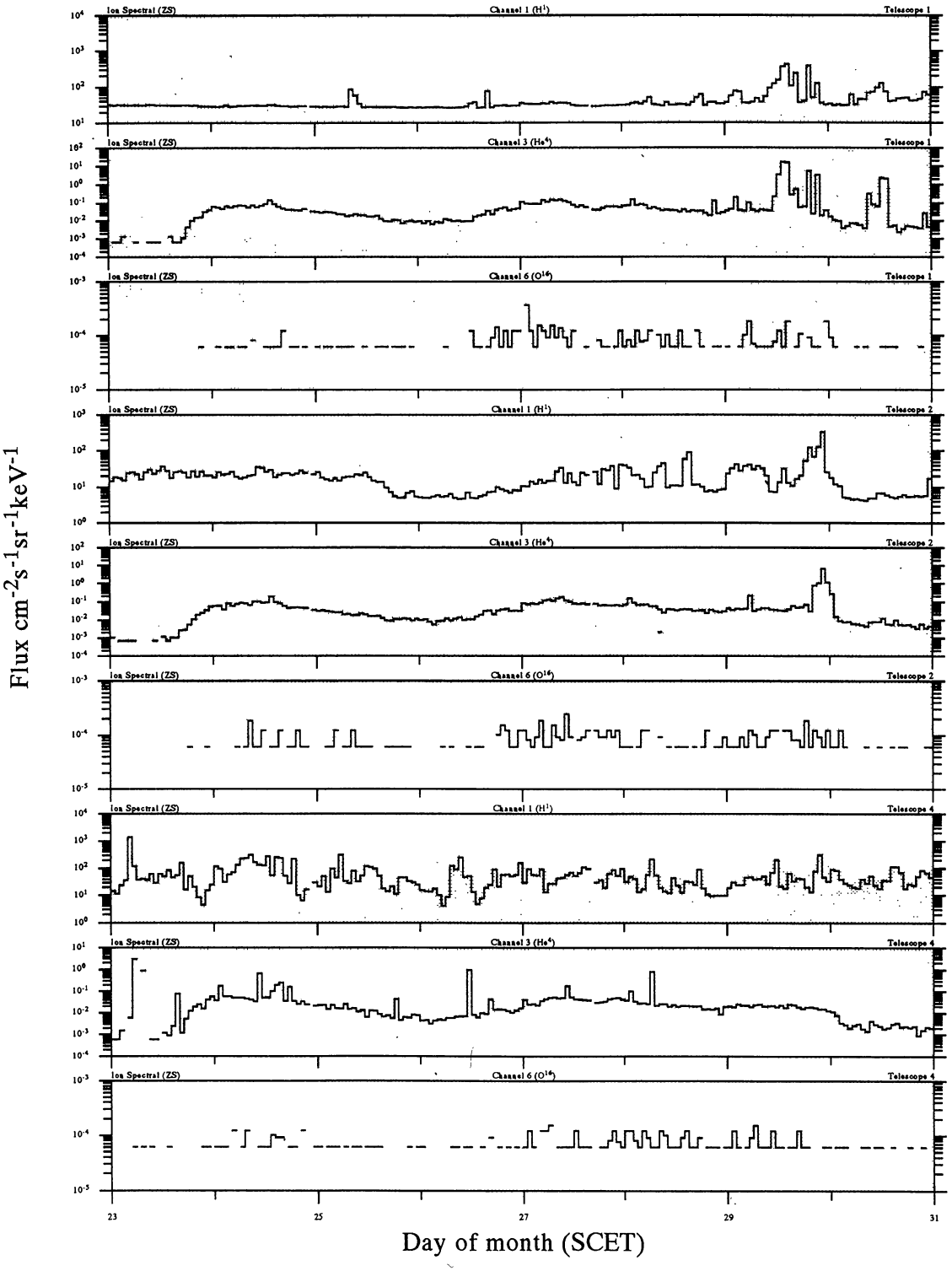

FIGURE 10. Ion channels 1 ($Z \geq 1$), 3 ($Z \geq 2$), and 6 ($Z \geq 6$) are shown for T1, T2, and T4. These channels correspond to protons, He and C-N-O. Hourly averages are shown.

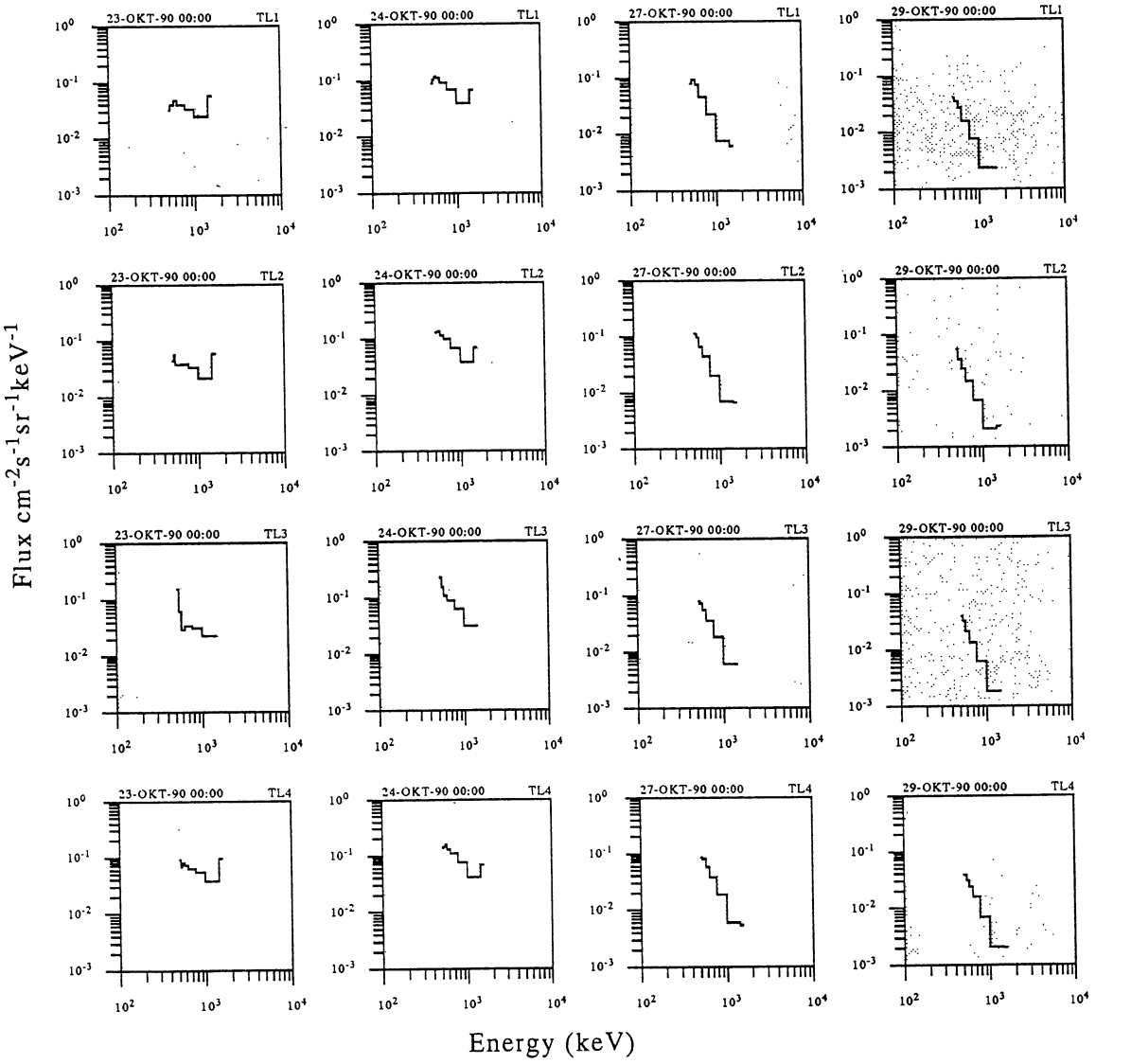

FIGURE 11. Energy spectra of protons (0.5-1.4 MeV) are shown obtained with the 4 telescopes during 4 days of the period 23 to 29 October 1990. Data represent daily averages.

ULYSSES-EPAC 23-OKT-1990 to 31-OKT-1990

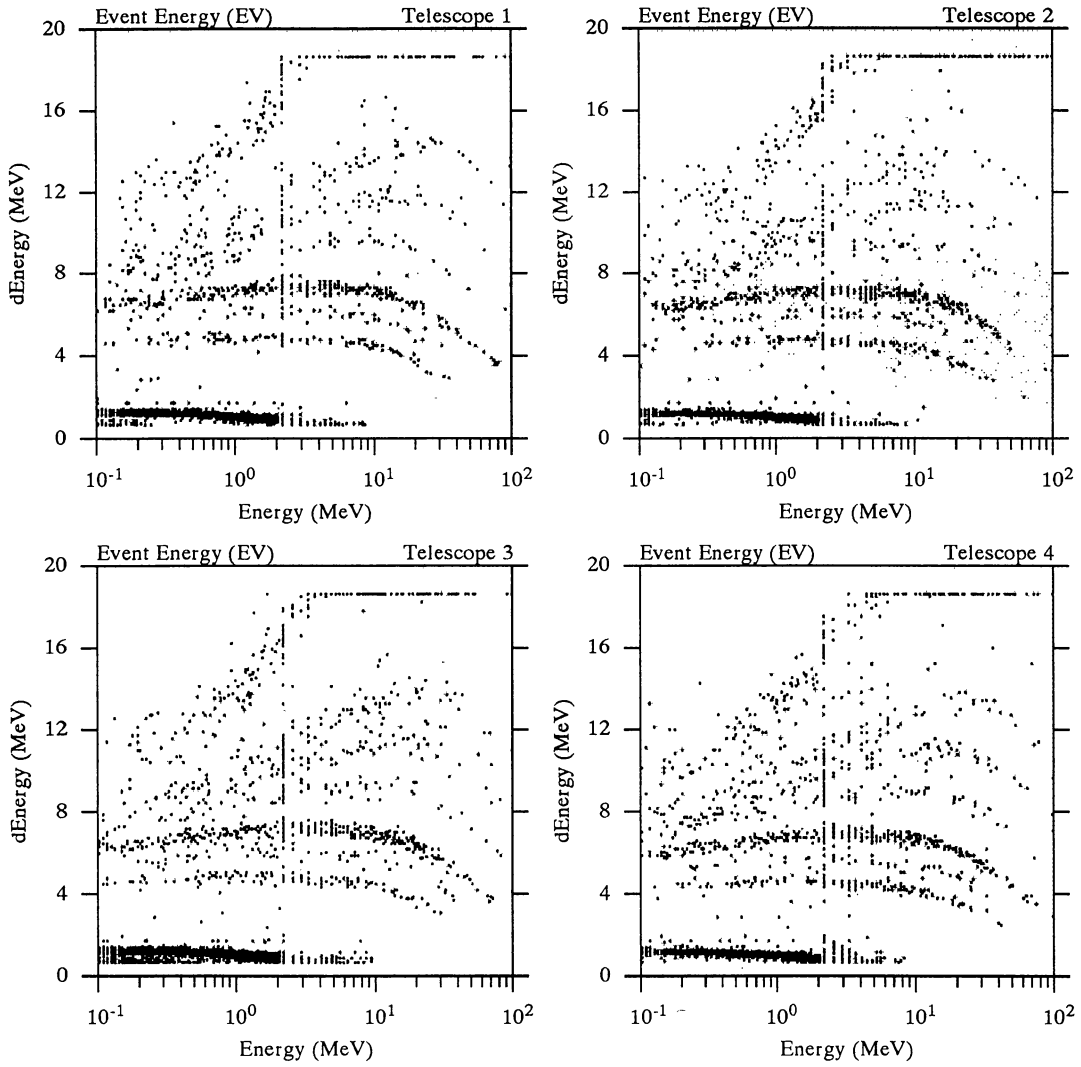

FIGURE 12. Events derived from a 2 parameter analysis are displayed. Energy loss in front-detector versus rest energy is shown. The gap near $E = 2$ MeV is an artifact due to an automatic range switch of the amplifier. Data are accumulated over the period 23 October to 29 October 1990. Protons are excluded; the lower track corresponds to He, next C-N-O tracks may be clearly seen and tracks due to heavier particles are also visible. The track indicated in the upper left part of the diagram corresponds to iron.